This is a repository copy of *Effect of plutonium doping on radiation damage in zirconolite: A computer simulation study*.

White Rose Research Online URL for this paper:
http://eprints.whiterose.ac.uk/79735/

Version: Accepted Version

eprints@whiterose.ac.uk
https://eprints.whiterose.ac.uk/

Effect of plutonium doping on radiation damage in zirconolite: a computer simulation study.

Henry R. Foxhall[a]*, Karl P. Travis[a] and Scott L. Owens[b]

[a] Immobilisation Science Laboratory, Department of Materials Science and Engineering, University of Sheffield, Sheffield S1 3JD, UK

[b] National Nuclear Laboratory, 5th Floor, Chadwick House, Warrington Road, Birchwood Park, Warrington, Cheshire, WA3 6AE, UK

* Corresponding Author
Henry Foxhall
Department of Materials Science and Engineering
Sir Robert Hadfield Building
Mappin Street
Sheffield, S1 3JD
U.K.

Email: h.foxhall@sheffield.ac.uk
Telephone: +44 (0) 114 222 6021

Abstract

We present the results of extensive Molecular Dynamics (MD) simulations of alpha-recoil radiation damage in a range of crystalline zirconolites, $CaZrTi_2O_7$. Our studied systems include pure zirconolite, which we use as a reference material and the first ever simulations of damage in Pu-doped zirconolite, where plutonium is doped onto both of the M1 sites in the material, i.e. $(Ca_{0.7}Pu_{0.3})ZrTi_2O_7$ and $Ca(Zr_{0.7}Pu_{0.3})(Ti_{1.7}Fe_{0.3})O_7$. Our goal was to determine the extent of local damage caused by a plutonium primary knock on atom (PKA) interacting with the crystal lattice. Recoil energies of up to 34.7 keV have been simulated. The damage is characterised using a number of analysis tools including: site specific radial distribution functions; defect statistics; and the asphericity parameter at various times during the annealing process. Our results show that there is much information to be gained by the use of novel techniques for radiation damage analysis. Also, we show inclusion of actinides in radiation damage simulations can significantly increase the extent of damage observed and should be considered carefully when describing radiation damage behaviour in future.

1.1   Introduction

SYNROC is the collective name for a family of multiphase ceramic wasteforms developed by Ringwood *et al.* [1] as candidate materials for immobilising rare earth elements (REE) and actinides (ACT). Containing three titanate phases: hollandite, zirconolite and perovskite, different formulations are designed to mimic naturally occurring crystalline rocks in which radioactive REEs and ACTs are found in solid solution and have remained stable over geological timescales, despite their propensity to amorphize as a consequence of repeated radiation damage from α-recoil events. In the UK, which has the world's largest stockpile of civil plutonium (*ca*. 110 tons) [2], a wasteform based on SYNROC-C in which zirconolite is the major phase is being considered for immobilisation of plutonium (Pu) residues through a processing route involving Hot Isostatic Pressing (HIPing).

For zirconolite to be used as a Pu host phase, a thorough knowledge of the mechanisms underpinning the amount of local damage sustained from alpha decay events, and more importantly, how and when the material recovers or heals, is of paramount importance. Current understanding is that the recoil atom from an alpha – decay, known as the Primary Knock on Atom (PKA) moves through the crystalline lattice, elastically colliding with other atoms and displacing them from their lattice positions [3, 4]. A succession of these cascades over a long period of time will lead to swelling and structural changes, which will have detrimental effects on the chemical and mechanical properties of the material, ultimately leading to reduced retention of actinides. Despite a good deal of experimental and theoretical studies into the behaviour of ceramics (including zirconolite) undergoing alpha damage [5-7] many puzzles remain. Open questions include: "why are some ceramics more resistant to radiation-induced amorphization than others?" and "of those ceramics which have undergone a crystalline to amorphous phase transition, why are some geologically stable?" Using topological arguments, we have recently begun to answer both of these questions, by analysing large-scale Molecular Dynamics (MD) simulations of alpha decay in models of zirconolite [8].

There have been many computer simulation studies of radiation damage in ceramic materials [9-14], but only a few concern zirconolite. Gilbert & Harding [15] and Mulroue *et al.* [16] have studied the energetics of individual defects and substitutions, but only a single previous study by Veiller *et al.* [17] has used MD to

investigate the intermediate-range effects of radiation damage in zirconolite. However, due to computer constraints, the recoil energies for Veiller *et al* were limited to < 12 keV, lower than the ~100 keV energy of a U recoil atom. Advances in computing (both in hardware and algorithms) have enabled both the simulation of more realistic recoil energies (requiring large system sizes > 1 million atoms) and long time scales (20 ps) are now commonplace, indeed MD simulations with billions of atoms will soon become routine. Using classical MD it is also possible to calculate the threshold displacement energy, E_d i.e. the amount of energy needed to permanently displace atoms from their lattice positions and form interstitial defects. These were calculated by Veiller *et al.* [17], where E_d ranged from 15 eV for oxygen, to 48 eV for Zr, comparing well with available E_d values from experimental observations. Their work also included an MD study of defect formation in cascades due to PKAs with energies between 2 and 12 keV.

Detailed experimental analysis of radiation damage in natural and synthetic zirconolite samples [5] has looked at many of the issues relating to their use as host matrices for Pu, but due to radiation protection and security issues laboratory-based research using Pu is difficult, costly and time consuming. Acknowledging previously published studies on Pu-containing zirconolite [18, 19], there is still a need for a greater understanding of how the presence of actinides changes the radiation behaviour and tolerance of a material. MD is a powerful tool in the quest for understanding of radiation damage as it has the ability to probe length and time scales unavailable to experimental analysis, adding weight to results of laboratory-based analysis. These time and length scales, at the picosecond and Angstrom level, happen to be almost exactly the time and length scales of radiation damage cascades. The first example of radiation damage MD is found in the work of Erginsoy *et al.* [20, 21], where the effects of radiation damage and recoil cascades in FCC Cu were studied. MD also has the advantage of not requiring the use of radioactive materials, which make it a comparatively cheap research method in the field of nuclear waste management.

The current authors feel that, building on the work of Veiller *et al.*, a more complete description of damage in zirconolite is now possible for three reasons: 1) The low recoil energies used by Veiller *et al.* do not fully represent the recoil energies seen in an alpha-recoil cascade and higher recoil energies are now more routinely possible due to computational advances, 2) There is a need for a more complete

analysis of the cascades on terms of size, shape and structure, and 3) The effect of actinide incorporation on the radiation damage behaviour of zirconolite must also be considered, but has thus far not been studied.

The present study further investigates alpha-recoil cascades in crystalline zirconolite with the aide of MD, using larger systems and higher recoil energies than Veiller *et al*. Calculations are presented on three materials: pure zirconolite, $CaZrTi_2O_7$, zirconolite doped with Pu onto M1 sites - $(Ca_{0.7}Pu_{0.3})Zr(Ti_{1.4}Fe_{0.6})O_7$ (where trivalent Fe acts as a charge balancing ion) and zirconolite with Pu doped onto M2 sites - $Ca(Zr_{0.7}Pu_{0.3})O_7$. These materials are termed Un-doped (UZ), Ca-doped (CAZ) and Zr-doped (ZRZ) zirconolite respectively. Our choice of model materials is based on research by Begg & Vance [22, 23], Deschanels *et al*. [24] and Gilbert *et al* [19] in which both groups found Pu to reside on Ca and Zr sites in their laboratory synthesized samples. Eight damage cascades in each material are assessed in terms of their atomic disorder, defect distribution, radial distribution functions, cascade size, and cascade shape. The residual damage is also taken into account. The simulations of alpha-recoil cascades in actinide-doped zirconolite are, to the authors' knowledge, the first published simulations of their type.

2.1 Methodology

2.1.1 Interaction potential

We have chosen the Buckingham potential [25] to represent atomic interactions in our simulations:

$$\phi_{BUCK}(r) = A\exp(-\rho r) - \frac{C}{r^6} \tag{1}$$

However, in radiation-damage simulations, high atomic kinetic energies can lead to ionic separations that probe the divergent region of the Buckingham potential giving rise to large, attractive, inter-atomic forces. We have therefore used a piecewise modified potential (described in detail below) where we use the Ziegler, Biersack and Littmark (ZBL) potential for short range interactions [26]

$$\phi_{ZBL}(r) = \frac{Z_i Z_j e^2}{4\pi\varepsilon_0 r} \sum_{k=1}^{4} c_k \exp\left(-b_k r / a\right) \tag{2}$$

where Z_i and Z_j are the atomic numbers of atoms with the labels i and j, ε_0 is the vacuum permittivity, $a = 0.88534a_0 \, (Z_i^{2/3} + Z_j^{2/3})^{-1/2}$ and a_0 is the Bohr radius The set of parameters: $\{b_k, c_k : k = 1,4\}$ is taken from the literature [26].

The Buckingham potential is used solely for separations exceeding its point of inflection (if present), or, if no dispersive term is specified, a convenient point for joining to the ZBL potential. The parameters used for the Buckingham potential were those obtained by Minervini *et al.* [27], collected together in Table 1.

Table 1: Buckingham potential parameters for atomic pairs in zirconolite [Minervini, 1999]

Atom pair	A (eV)	ρ (Å)	C (eV Å^6)
O – O	9547.96	0.21916	32.0
Ca – O	784.38	0.36356	0.0
Zr – O	1502.11	0.3477	5.1
Ti – O	2131.04	0.3038	0.0
Pu – O	1762.84	0.3542	11.48
Fe – O	1414.60	0.3128	0.0
Cat - Cat	0.0	1.0	0.0

The two potentials must be joined, and many methods exist in the literature. Switching functions provide an exponential decay of one function into the other [28] while the use of mathematical splines matches the ends of the two potentials [10]. Some researchers have eliminated the need for a specific short range potential and joining function completely through manipulation of the dispersion terms of their potential - allowing atoms to be closer before such potential catastrophes occur, making them highly unlikely [12]. It is our view that a representation of the close-range forces should be based on the close range properties of atoms, as detailed by the ZBL potential, and that an equilibrium Born-Mayer potential form is not suitable for this application. We have chosen to use a cubic spline, which ensures both the energy and forces in an MD simulation are smooth and continuous. The spline fitting was carried out using an algorithm described in Numerical Recipes in Fortran [29]. The potentials defined in (1 & 2) were tabulated at a number of points along the two

intervals: $[r_1,10]$ and $[0, r_0]$ respectively using a grid spacing of 0.002 Å. In this work we took $r_0 = 0.6$ Å and $r_1 = 1.0$ Å for all interactions except O-O and Zr-O, for which $r_1 = 0.88$ Å. The spline fitting was performed on the range $[r_0, r_1]$, and tabulated using the same grid spacing as above, where the cubic spline potential is defined by

$$\phi_{SPLINE}(r) = \sum_{k=0}^{3} p_k r^k \tag{3}$$

The composite potential is therefore

$$\phi_{COMPOSITE}(r) = \begin{cases} \phi_{ZBL} & r < r_0 \\ \phi_{SPLINE} & r_0 \leq r \leq r_1 \\ \phi_{BUCK} & r > r_0 \end{cases} \tag{4}$$

The Coulombic contribution to the potential energy, ϕ_{COUL}, was evaluated by DL_POLY using the smooth particle mesh Ewald sum method [30] and thus is not included in the main composite potential. The total pair energy is therefore:

$$\phi_{TOTAL}(r) = \phi_{COMPOSITE} + \phi_{COUL} \tag{5}$$

The Ewald convergence parameter (width of the Gaussian charge distribution) was taken to be 0.28461 Å^{-1}, based on a target precision of 1×10^{-5} and kmax1 = kmax2 = kmax3 = 128. All MD simulations in this work were conducted using the package DL_POLY 3.06 [31].

2.1.2 Unit cell structure

Zirconolite is a superstructure based on an anion deficient fluorite ($CaF_{2-x}Mo_{2-x}$). It has a monoclinic structure with alternating layers of Ca/Zr ions and Ti ions. The Ti layer comprises a hexagonal tungsten bronze (HTB) arrangement of mainly corner-sharing [TiO_6] octahedra [32]. An initial 2x2x2 supercell configuration was created using the fractional coordinates according to Rossell and used as input to the GULP (General Utility Lattice Program) code [33]. GULP internally handles partial occupancies in a statistical manner, so those described by Rossell were included (7% Ti substituted on the Zr M2 site and 14% Zr substituted on the Ti M4 site). A Newton-Raphson energy minimisation with full relaxation of the cell size and shape was performed using the standard Buckingham potential as described in Table 1. The

calculated lattice parameters were found to differ by less than 2.5% from the values obtained by Rossell (see Table 2) and the density was reproduced to an acceptable level. Phonon spectra were calculated and no negative frequencies were found.

Table 2: Comparison of calculated crystal unit cell parameters with experimental data for zirconolite.

Parameter	Experimental value [Rossell, 1982]	Calculated value	Difference (%)
Volume (Å^3)	1014.0604	999.3713	-1.45
a (Å)	12.4458	12.1417	-2.44
b (Å)	7.2734	7.1538	-1.64
c (Å)	11.3942	11.6781	2.49
α (deg)	90.000	90.000	0.00
β (deg)	100.533	99.857	-0.67
γ (deg)	90.000	90.000	0.00
Density (g/cm^3)	4.7	4.507084	-4.10

For MD simulations, where statistical representation of partial occupancies was not available, cation species were swapped on randomly chosen M2 and M4 sites until the required partial occupancies were met. This process took place *after* the supercell had been created, ensuring no replication or periodicity of substitutions was present in the simulation cell. Supercells used in this work were 4x4x4 (5632 atoms) for physical property calculation and 12x18x12 (228 096 atoms) for radiation damage simulations. Ideally, a cubic system would be used to maximise the number of directions in which cascades could be simulated with sufficient box size, and the latter cell was designed to meet this requirement as closely as possible given the monoclinic nature of the unit cell.

Further validation of the chosen potential was sought by calculation of the bulk modulus. A series of equilibrium NpT runs on a 5632 atom system were conducted at 300 K, for a set of applied pressures ranging from 300 to 1000 atm. The time-averaged simulation volume was obtained from each simulation and found to

vary linearly with applied pressure. The bulk modulus (inverse isothermal compressibility) was then estimated using

$$\kappa_T^{-1} = -V \left(\frac{\partial p}{\partial V} \right)_T , \tag{6}$$

where k_T is the isothermal compressibility, evaluated at the volume of the energy-minimised simulation cell, i.e. $V = 27.094$ nm^3 for a 5632 atom system. We obtained a bulk modulus value of 235 GPa. While we have been unable to source a published value for the experimentally obtained bulk modulus of zirconolite, our estimated value compares favourably with that of 224.3 GPa, calculated by Veiller et al. [17]. Both these values are of comparable magnitude to published experimental values for other crystalline oxide ceramics (e.g. 186 GPa for $Gd_2Ti_2O_7$ [34], and 225 GPa for zircon, $ZrSiO_4$ [35]), providing further confidence that the potential model used is reasonable.

Doping of Pu atoms into the system was performed as described above (for partial occupancy creation) with substitutions made up to 30% of the Ca(M1) or Zr(M2/M4) atoms. As before this was performed after creating the supercell. In systems where Pu was doped onto a Ca(M1) site, charge balance was achieved by doping trivalent Fe ions onto Ti(M3) sites, a substiution commonly found in geological zirconolite samples.

2.1.3   Cascade simulations

In all simulations, a Pu (rather than U) atom was used as the recoil atom, greatly simplifying the simulations by minimising the number of atomic interactions necessary in the simulation input files. To prevent atomic interactions passing through the periodic boundaries, a stochastic Langevin thermostat was applied to the outer 3 Å of the simulation cell using the preset DLPOLY 'pseudo layer' thermostat as detailed in the DLPOLY manual [36]. A Pu atom was then selected from the next 7 Å of simulation cell (i.e. a layer between 3 and 10 Å from the very edge of the simulation cell) to become the primary knock-on atom (PKA). The components of its velocity were altered such that the kinetic energy equalled 34.7 keV, with the direction of travel obtained by choosing a unit vector sampled the octant of a unit sphere (centred at the cell corner) contained within the simulation cell.

Radiation damage simulations employed a variable time step integration algorithm with an initial time step of 5 x 10^{-6} ps, which was modified after each timestep so that the maximum displacement of an atom was between 0.01 and 0.05 Å per timestep. A typical 75000 time-step simulation equated to 28 ps of simulation time.

3.1 Results and Discussion

In what follows, we use standard Kröger - Vink notation for defects, M_S^C, where M is the species, e.g an element or vacancy defect V, S is the lattice site on which it resides, and C is the charge of the defect relative to the initial site, either negative, positive or neutral represented by ', • and × respectively.

3.1.1 Analysis of Cascades – Un-doped Material

Upon introduction of a recoil atom, defects rapidly increase in number due to the large number of atomic collisions. A visualisation of the evolution of a typical damage cascade is shown in Fig. 1, where atoms appear only if they have moved a distance > 0.8 Å from their initial positions (0.8 Å was chosen to facilitate comparison with the work of Veiller *et al*. [17].
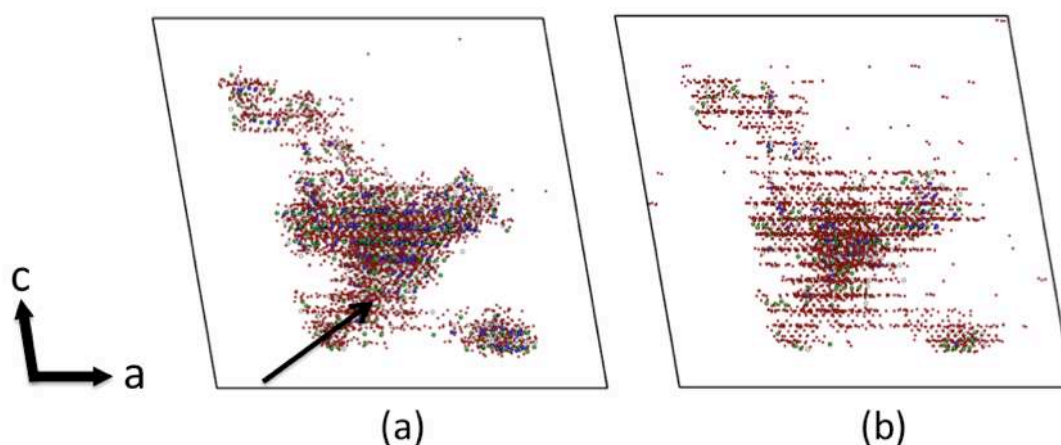

Figure 1:   Simulation snapshots showing damage in UNZ at elapsed times: (a) 0.4 ps and (b) 1.5 ps. The arrow indicates the initial direction of the PKA.

At its maximum size, the cascade contains several thousand atoms, but this number decreases before reaching some asymptotic value, indicating a strong degree of self-healing, evident from Fig 1b taken 1.5 ps after the recoil event. Many atoms return to their respective sub-lattices and remain in the visualisations in Figure 1b because the sites on which they now reside are not those on which they started. Distinct lines of oxygen atoms are visible due to Frenkel pair recombination ($O_i'' + V_O^{\bullet\bullet} \rightarrow O_O^{\times}$) along the HTB layers – highlighting increased structural rearrangement in these areas. We have shown in previous work [8] that there is significant polymerisation of the [TiO_x] polyhedra during radiation damage in zirconolite, and that observation is further evidence of this phenomenon. In close proximity to the PKA track, significant disruption of the crystalline lattice is seen, with large numbers of atoms moving away from their reference crystal site as a result of either physical collisions or from thermal effects due to an energetic shockwave that propagates through the system. Directly around the PKA track, atoms are moved the furthest and are least likely to return to their initial atomic positions as many travel distances greater than the inter-atomic distance in zirconolite. In this case, atoms will either find a suitable lattice site to occupy and form an antisite defect, or remain as an interstitial ion. In Fig. 1a & b, one also sees propagation of damage far into the crystal in a direction perpendicular to that of the initial PKA, as well as continuing in the direction of the PKA. Qualitatively this can be described as 'splitting' of the damage cascade by formation a secondary knock-on atom (SKA), forming sub-cascades that can propagate a significant distance through the lattice.

Changes in gross crystal structure are often analysed by means of the radial distribution function, g(r). Figure 2 shows the O-O g(r) of the equilibrium crystal (pre-damage) and 0.8 ps of elapsed time after the recoil event. The effect of a single damage cascade on the overall atomic structure of the simulation cell is small due to the small percentage of atoms in the entire system involved in the damage cascade. There is evidence of a change in the short-range structure at values of *r* between 3.5 and 4.5 Å, and also some moderation in the intermediate-range structure (8-9 Å).
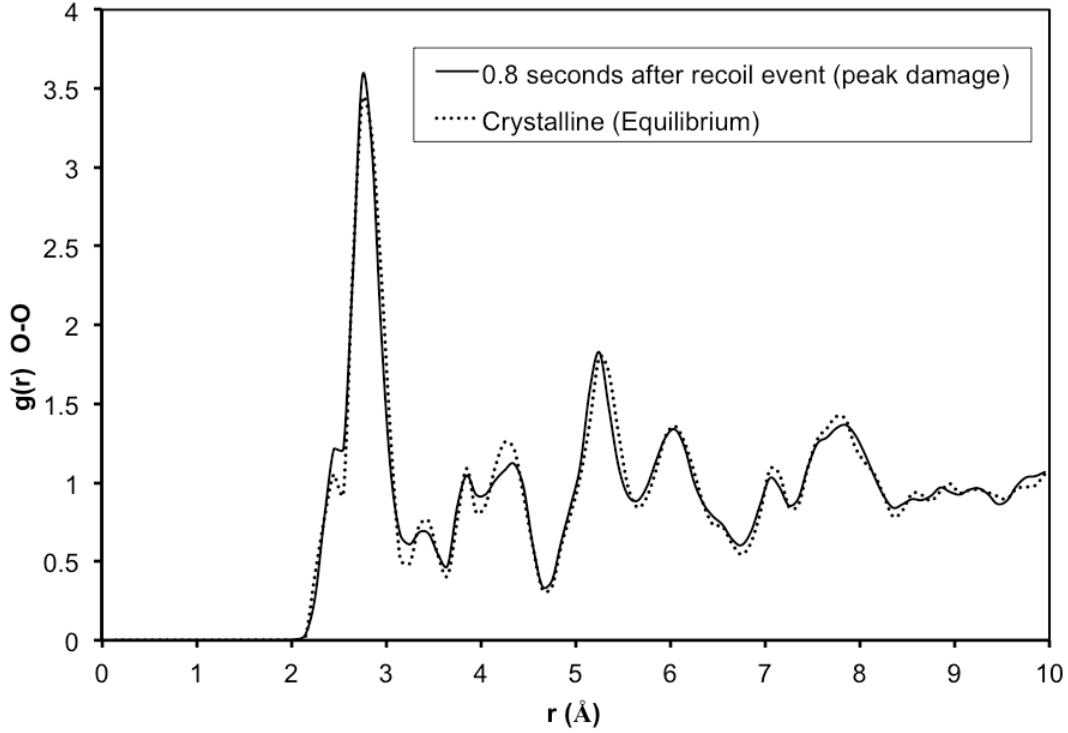
Figure 2: Partial (O-O) radial distribution functions for the crystalline (undamaged) UNZ and 0.8 ps after introduction of the recoil nucleus, the point at which the defect population was at its largest.

The simulated cascade and consequently damaged volume of zirconolite may also be conveniently discussed in terms of a defect lattice structure. Three categories of defect are thus analyzed: antisite defects, vacancies and interstitials. An antisite defect is defined as an atom occupying an atomic site other than its initial lattice position; an atom moving to occupy a stable interstitial site from its initial lattice position creates a vacancy; and an interstitial defect is an atom not occupying any defined lattice site. The number and type of such defects was monitored during simulations relative to the initial energy-minimised structure. As the PKA begins to interact with the system some atoms will either temporarily or permanently leave their lattice sites and create defects. If the initial and final atomic positions x and y are points in the usual space, R^3, such that $x = (a_1, a_2, a_3)$ and $y = (b_1, b_2, b_3)$, and $D(x, y)$ is the usual Euclidean metric defined by

$$D(x,y) = \sqrt{(a_1 - b_1)^2 + (a_2 - b_2)^2 + (a_3 - b_3)^2} ,\qquad (7)$$

we may then represent the cascade as a point set, C, in the following way,

$$C = \{x : D(x, x_0) > \delta\} \tag{8}$$

where x_0 is a reference point (lattice site at time $t = 0$) and δ is an arbitrary tolerance. Clearly $C(t = 0) = \varnothing$, since all atoms then reside on their lattice sites. At times t > 0, the atoms may have moved a radial distance from their lattice sites which exceeds the tolerance and hence their spatial positions are then members of the cascade set. The members of this set will vary with time as the cascade develops and the crystal heals. Atoms returning to their initial positions are removed from the set, but atoms returning to a lattice site *other* than their original remain in the set, as they remain displaced from their time zero position.

The absolute number of calculated defects is evidently a function of δ, however, qualitative cascade behaviour was found to be insensitive to this tolerance value. The time-dependant behaviour of the defect population during a cascade highlights two distinct regimes for local damage production; a highly non-equilibrium phase where the significant part of the energy from the PKA is elastically transferred to the lattice, and a post-cascade phase in which relaxation of the structure occurs without significant transfer of energy through the crystal. Multiple simulations of single 34.7 keV cascades with varying initial recoil directions in UNZ showed wide variations in behaviour, with defect populations peaking at times between 0.3 and 0.5 ps. The individual populations numbered between 2817 and 12253 with an average of 8489 and are plotted with respect to time in Figure 3, which highlights large variations in behaviour depending on the position and direction of the initial recoil atom.
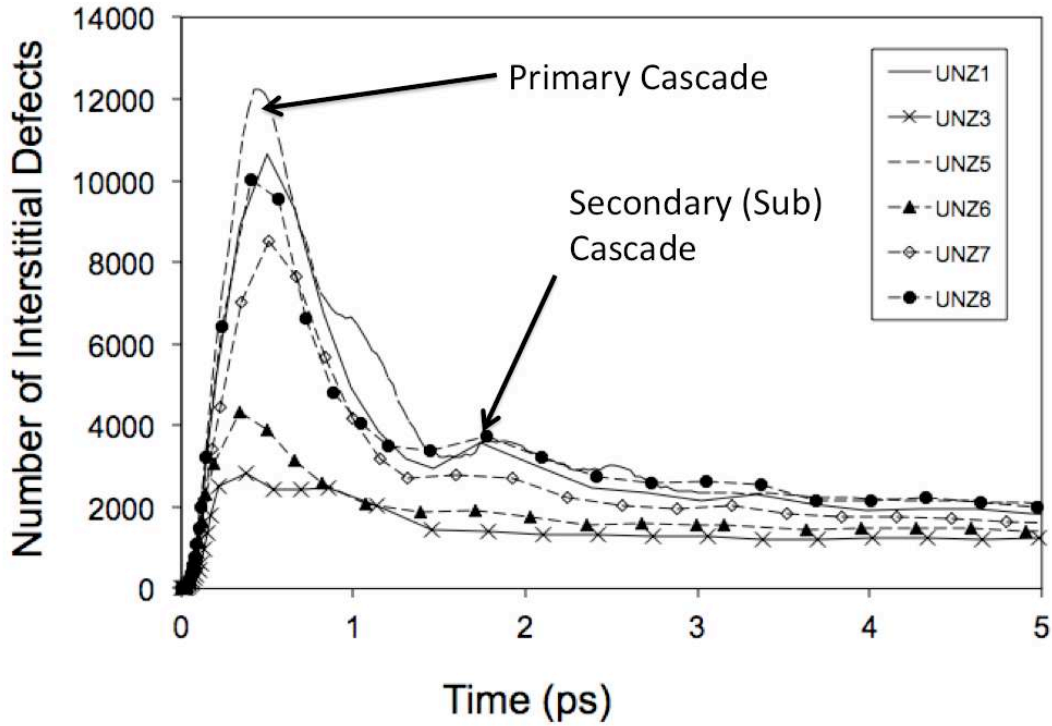
Figure 3: Plot of the total number of displaced atoms in UNZ versus time elapsed since introduction of a 37.4 keV recoil event for 6 PKA atoms in randomised directions. The recoil nuclei all had initial energies of 37.4 keV.

In some cascade simulations, where later on in the cascade a very intense collisional transfer of energy occurs between two zirconium ions (i.e. the heaviest ions in the UNZ system), a sub-cascade occurs - revealed as a secondary peak in the defect population at $t \approx 1.8$ ps. There were only a few small sub-cascades seen in UNZ, and with the heaviest possible SKA being a Zr ion – with only around 40% of the mass of a U ion – their track and penetration through the crystal lattice was small.

After the highly non-equilibrium shock wave subsided (around 2 ps after the introduction of the PKA), a large proportion of atoms meet the criterion $D(x,x_0) < \delta$, signalling an end to this portion of the damage cascade. The system then continues to anneal, with a small amount of defect recombination occurring. After 25 ps, remnant defects number between 1173 and 2660 for the set of UNZ simulations. On average, there are 1621 remnant defects in UNZ, mostly Frenkel pairs $\left(V_O^{\cdot\cdot} + O_I'' \right)$ due to displaced oxygen atoms. Despite very large variations in peak numbers of displaced atoms, the spread of results reduces with simulation time, suggesting the effect of the shockwave size is less than may initially be suggested by the peak numbers of defects. Results were consistent with those by Veiller who observed a thermal spike initially

displacing around 10000 atoms 0.8 Å from their zero-time positions for a 12keV PKA.

Gilbert and Harding [15] found that many antisite defects are energetically unfavourable with respect to a perfect crystalline zirconolite lattice, suggesting that some are highly unlikely to form under equilibrium conditions. However, we are observing a re-arrangement of atoms under highly non-equilibrium conditions during radiation damage, therefore the formation of all antisite permutations is possible (permutations, as Ca''_{Ti} is not the same as $Ti^{\cdot\cdot}_{Ca}$).

Fig. 4a shows the variation with time of the antisite defect population. An increase in antisite numbers occurs up to $t = 4$ ps before plateauing around 2700 antisite defects. To further understand the changes taking place it is instructive to consider the numbers of individual antisite defect permutations, plotted, for simulation UNZ_1 as a function of time in Fig. 4b (cation-cation pairings) and Fig. 4c (cation-O pairings). The graphs show that, with no more than 50 antisite defects for any cation pair, and 283 Cat_{Cat} antisites in total, this defect type accounts for only 11% of the defect population. Cat_{cat} antisites of varying charge states, while small in number, follow the same qualitative behaviour as the total number of antisite defects. It is likely that Cat_{Cat} antisite defects remaining after the highly non-equilibrium period of the cascade will remain stable for long periods of time (subject to a lack of interaction with further alpha-recoil cascades) due to the energy needed to remove a cation from its resident site, metastable or otherwise. Ca_{Ca} antisites are most numerous, while Zr_{Zr} antisites are rare. This is not surprising, given Veiller *et al.* used a Buckingham/ZBL composite potential and MD to calculate the threshold displacement energies (E_d) for ions in zirconolite and found Ca ions to have a value half that of Zr ions, citing 25 and 48 eV respectively for the amount of energy needed to displace each ion type from a lattice site. All Cat_O antisite defects are transient, peaking between 0.2 and 0.7 picoseconds before vanishing altogether, with Ti_O defects dominating briefly at short times, unsurprising given the high numbers of oxygen atoms associated with [TiO$_x$] polyhedral re-arrangement in the HTB layer [8]. Therefore $O^{\times}_O$ defects account for ~90% of all antisite defects seen. That these antisite defects dominate overall is also to be expected on statistical grounds given that there are many more oxygen atoms and hence oxygen sites for Frenkel pair recombination. These defects cause no net observable change to the system.
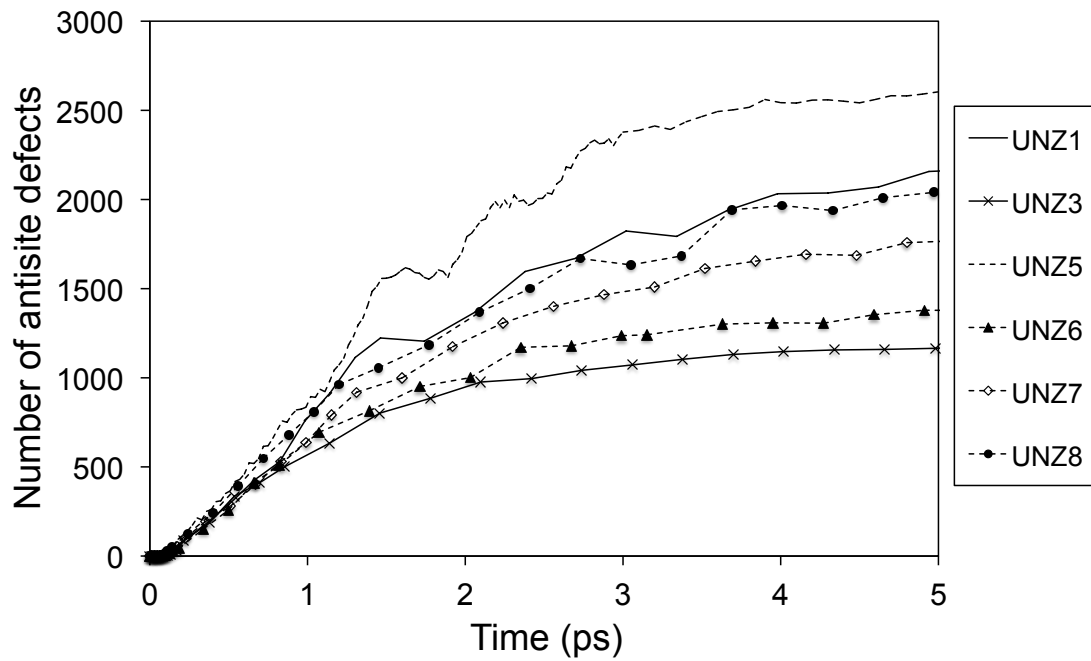
15

Figure 4a: Plot of total number of antisite defects versus elapsed time since introduction of a 37.4 keV recoil nucleus for 6 separate cascades in UNZ.
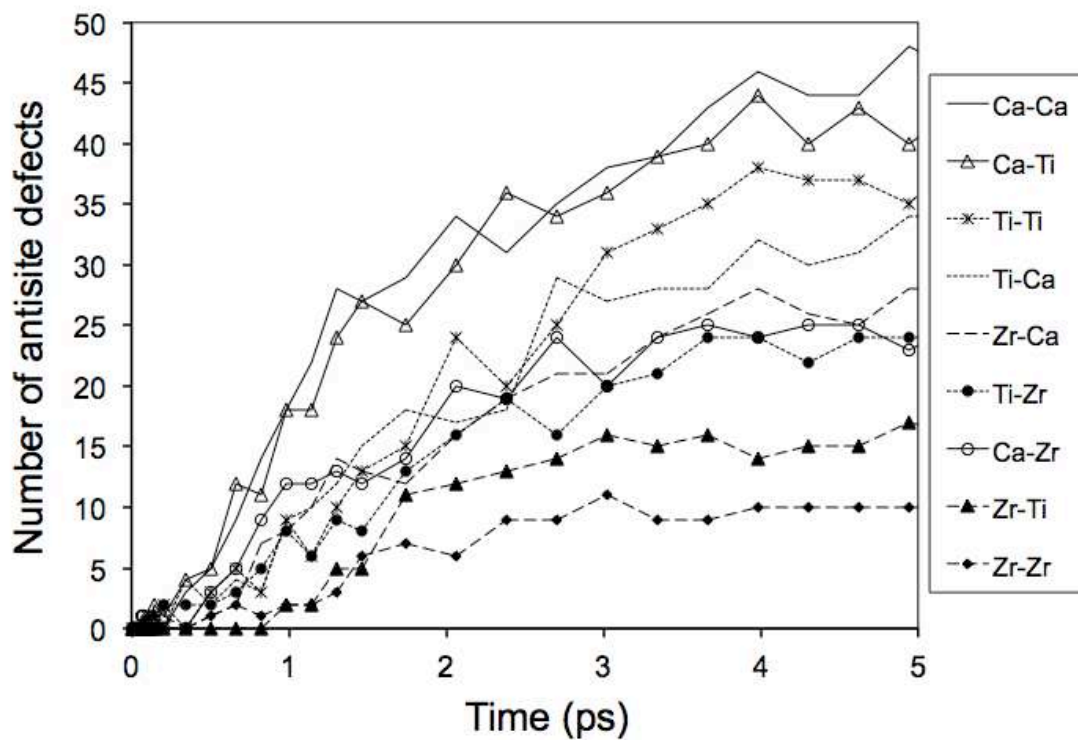

Figure 4b: Plot of Cat_{Cat} antisite defects for UNZ as a function of elapsed time since the introduction of a 37.4 keV recoil nucleus.
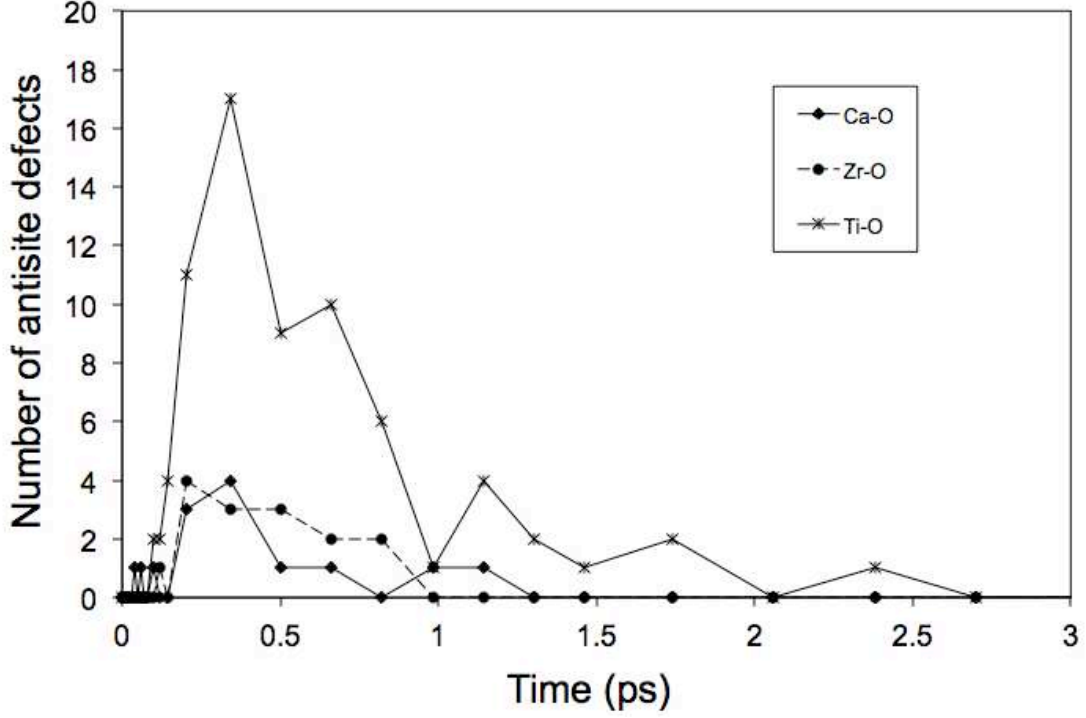
Figure 4c: Plot of the average number of Cat_O antisite defects as a function of time since the introduction of a 37.4 keV recoil nucleus.

The geometry of the evolving damage cascade may be discussed in terms of its radius of gyration and relative shape anisotropy, which can be represented with an asphericity parameter, according to Dunn *et al.* [37]. Both of these quantities can be obtained from the "inertia" tensor, $\boldsymbol{\Theta}$, defined by

$$\Theta = \frac{1}{N}\sum_{i}^{N}(x_i - x_c)(x_i - x_c) \tag{9}$$

where $\boldsymbol{x}_i$ is the position vector of atom i in the cluster and $\boldsymbol{x}_c$ is the geometric centre of the cluster. For example the mean square radius of gyration may be obtained from the trace of the diagonalized form of this tensor,

$$R_g^2 = \sum_{i=1}^{3}\lambda_i \tag{10}$$

where the λ's are the eigenvalues of $\boldsymbol{\Theta}$. The asphericity parameter [37] is defined by,

$$A = \frac{\sum_{i<j}^{3}(\lambda_i - \lambda_j)^2}{2R_g^4} \tag{11}$$

and has a range [0, 1], representing spherically symmetric objects and elongated or 'cigar' shaped clusters respectively.

17

Taking the mean squared radius of gyration first (Figure 5), we find that cascades have values ranging between 1400 and 2200 Å^2, and the square root of this value represents the size of cascade interaction volume; 37 – 47 Å. This characteristic size is much smaller than the length of the cascade (defined here as the longest distance measurable in the region where atomic displacement > 0.8 Å) which for all simulations was > 100 Å. The width of these regions using a similar criterion was 40 - 70 Å, so the radius of gyration appears to be a reasonable estimate of the cross sectional diameter of a cascade.
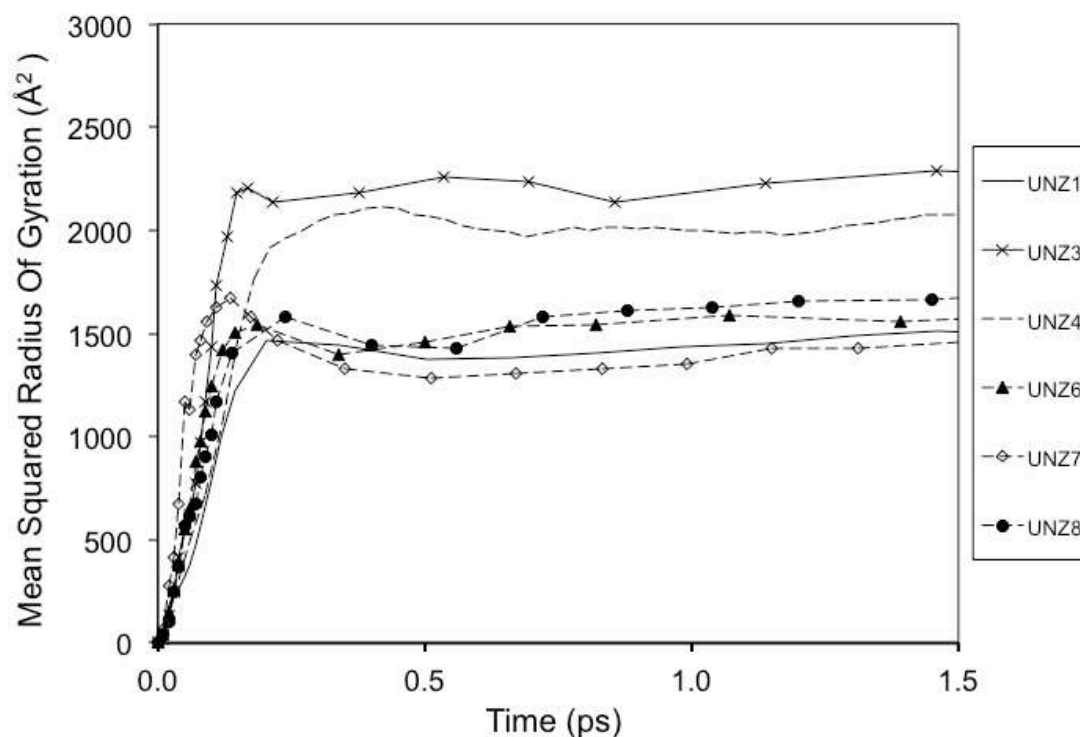

Figure 5: Plot of the mean squared radius of gyration (defined by Eq. 10) versus time for the evolving UNZ damage cascades.

Asphericity values for clusters of atoms involved in cascades averaged 0.271, suggesting egg-shaped cascades. However, asphericity values ranged from 0.040 to 0.608, as seen in Figure 6, so it is misleading to consider this result due to the large spread of values. This quantitavely confirms the visual observation of large variations in cascade shape due to variations in initial PKA position and recoil direction.
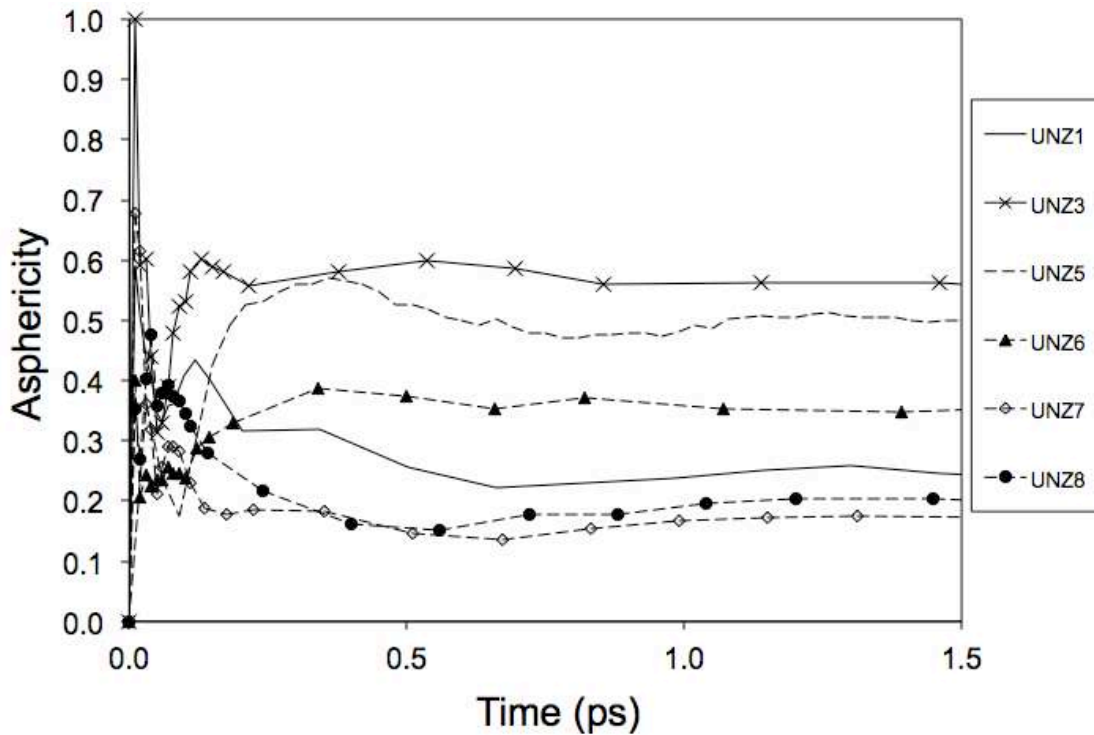
Figure 6: Plot of asphericity parameter (defined by Eq. 11) versus time for the evolving UNZ damage cascades.

3.1.2 Analysis of Cascades – Doped materials.

The first step for comparison of cascades in UNZ, ZRZ & CAZ is visualisation, and significant differences are seen in all cases. In ZRZ, up to 10 sub-cascades were observed in a single simulation – a substantial increase from the UNZ simulations. Each sub-cascade was small in volume, but due to their larger numbers the overall damage region extended much further into the simulation cell, as shown in Figure 7. The large range of the sub-cascades allow the effects of radiation damage to spread much further through the material even though the number of atoms involved may not actually have increased (discussed later).
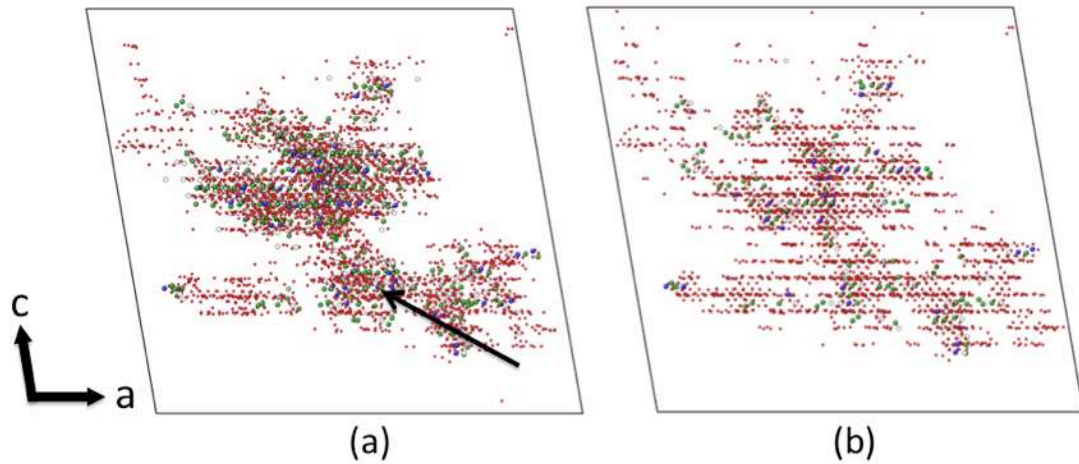
Figure 7: ZRZ simulation snapshots (from ZRZ2), showing (a) maximum and (b) residual damage, at 0.4 and 1.5 ps respectively, viewed along the *b* unit cell direction. The initial direction of the 37.4 keV PKA is arrowed.

In CAZ simulations, sub-cascades numbered similar amounts to the UNZ simulations but were much larger in volume than any seen in either ZRZ or UNZ systems. Examples of this behaviour are shown in Figure 8, where it can be seen that in CAZ simulations the sub-cascades involve large numbers of atoms and also a larger volume of affected crystal. In order to quantify these visual differences, one can once again turn to monitoring defect populations. Initially, formation of defects and displacement of atoms occurred at the same rate for all three systems in this work.

In ZRZ material the average peak time of the thermal shockwave is almost identical to that in UNZ simulations at 0.43 ps, with times ranging between 0.30 and 0.51 ps. Peak defect numbers however were spread over a smaller range, shown in Figure 9. For ZRZ, vacancy numbers lie between 4398 and 10725 with an average of 6454, thus there are around 25% fewer vacancies formed than in the UNZ material. By the time the thermal shock has subsided, the remaining vacancies are similar in number to the UNZ simulations, with an average of 1546 residual vacancies.
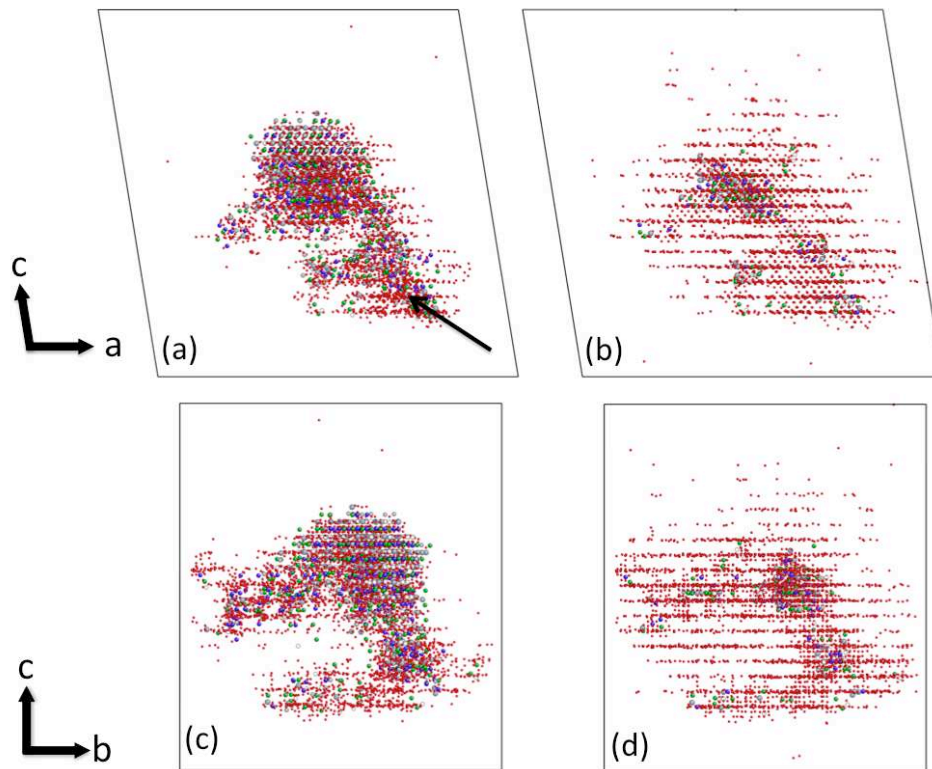
Figure 8: Typical CAZ simulation snapshots (from CAZ6), showing (a,c) maximum and (b,d) residual damage at 0.4 and 1.5 ps respectively, viewed along the *b* (Fig a & b) and *a* (Fig c & d) unit cell directions. The initial direction of the 37.4 keV PKA is arrowed.
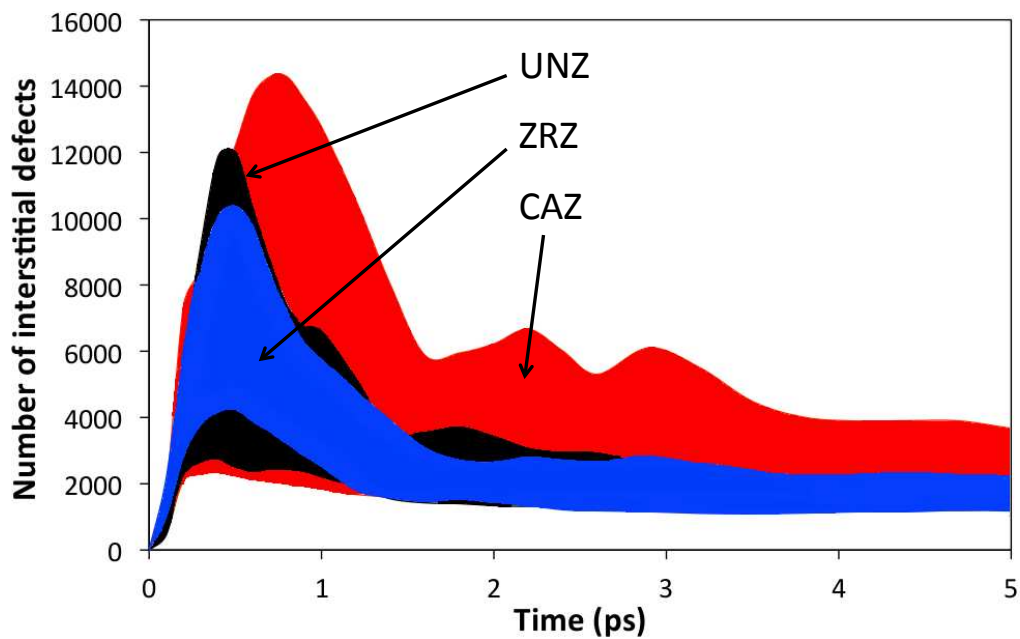

Figure 9: Plotted maximum and minimum numbers of atomic displacements > 0.8 Å for all simulations on UZ, ZRZ & CAZ.

The peak atomic displacement seen in simulations with Pu doped on to the Ca sites occurred later, and was much greater in magnitude than in UNZ simulations; between 0.35 and 0.94 ps, with an average time of 0.65 ps. The length of the cascade was longer with significant changes in defect numbers seen through until 3.5 ps, with multiple and sizeable sub-cascades also observed in this time, as the possibility of a Pu SKA means that much heavier ions are involved in collisions throughout the cascade. Most notably this was seen in the CAZ systems, leading, in two simulations, to large secondary peaks in the number of vacancies formed, and very large volumes of crystal being affected by the radiation damage event.

The antisite defect population over time is plotted for the three materials in Figure 10. Doping Pu onto the Zr or Ca sites appears to affect the material in different ways, with less disruption to the CAZ lattice. This is contrary to what would be expected as for CAZ systems, given the much larger number of atomic displacements seen and the larger region of crystal affected by the radiation damage cascades, one would expect antisites to be more numerous. This suggests either a disinclination for interstitial cations to recombine with nearest atom sites, preferring to remain as interstitial ions in the system, or a strong tendency, for instance, for Ca atoms to return to Ca sites. Transient numbers of antisite defects in the systems were comparable in all three systems, and there were an average 52.0 and 37.7 remnant Cat_{Cat} defects in ZRZ and CAZ respectively, compared with 63.1 for UNZ simulations. Both sets of simulations therefore were subjected to less residual cation disorder than the UNZ material.
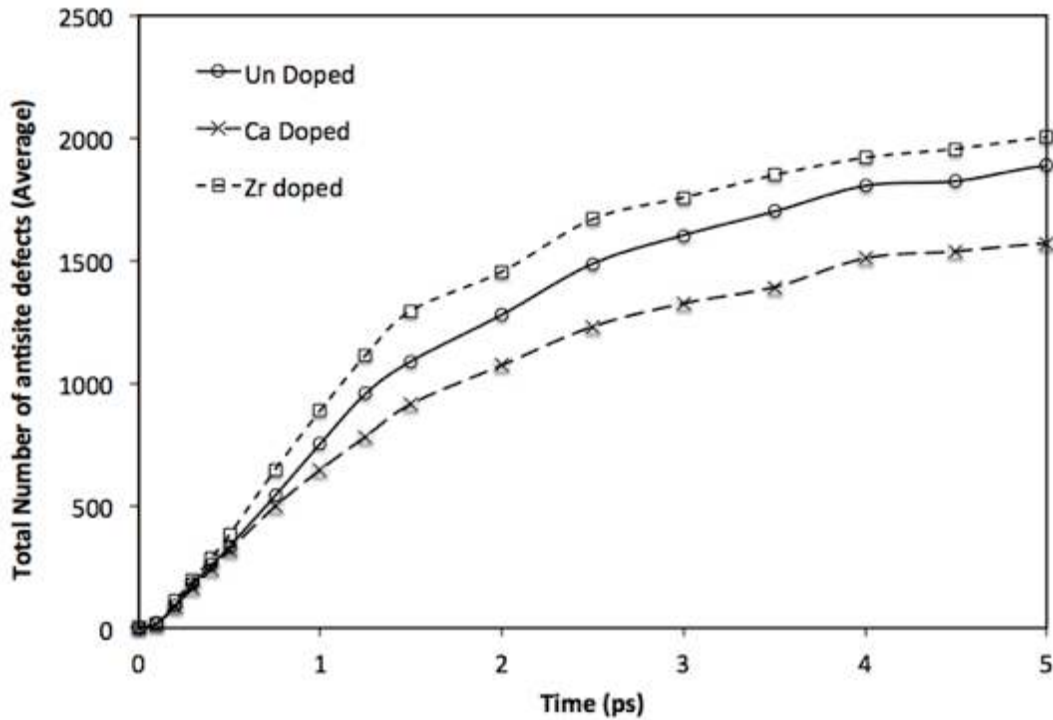
Figure 10: Plot of average antisite defects as a function of time since introduction of the recoil event. The recoil nucleus had an initial energy of 37.4 keV

There are similar variations and spread in the asphericity of ZRZ and CAZ cascades when compared to UZ. Values averaged 0.274 and 0.326 for ZRZ and CAZ simulations respectively (compared with 0.271 for UZ) and suggest that cascade shapes are similar in all materials, with CAZ cascades potentially being slightly more elongated. However, visualizations such as figures 7 and 8 show that this is not necessarily the case, and very little correlation is seen in cascade shape. The authors would hesitate to make any prediction on cascade shape trends from these distributions.

Radius of gyration values are similarly unchanged for ZRZ and CAZ cascades, suggesting that despite the large variations in atoms involved in cascades, the actual volumes of affected crystal are similar, and that the damage in CAZ is more densely packed.

4.1   Conclusions

The work presented here has greatly extended the analysis (both qualitative and quantitative) of radiation damage simulation in ceramics beyond what currently exists in the open literature. In pure un-doped zirconolite, significant differences have been shown to exist in cascade behaviour depending on initial starting recoil direction. This would suggest that statistical confidence in damage cascade results must be improved through performing as many simulations as is reasonable, since every one is likely to be different. In this work we performed at least 6 cascades in each material, similar in all but their initial recoil direction, and the authors' preference in future work would be increase this further, as results here suggest that consideration of the initial direction of the recoil atom is vital to descriptive results of damage behavior in materials. There has been a tendency for previous authors to maximize the distance available for cascade propagation by giving the recoil atom an initial [111] direction. With this being such a defined crystallographic direction in many materials, we would suggest that this choice would minimize the variation in results obtained, and therefore conclusions that can be drawn, to a small percentage of what would ideally be possible.

The simulations of alpha-recoil cascades in doped material are to our knowledge the first of their kind, and highlight the behavioural differences between doped and un-doped material. The results suggest damage behaviour is significantly altered by the presence of heavy dopant ions such as Pu, and their availability as secondary knock-on atoms means the number of sub-cascades is larger and cascade size increases. The consequences of this are far reaching – ion bombardment experiments to assess radiation damage accumulation in pure materials may underestimate the extent of damage and the physical and mechanical effects on the material may be more serious than first thought.

In terms of the techniques used for analysis of radiation damage in molecular simulation, use of a reference cell method has its limitations. It will significantly over-estimate the size of the observed damage region since during the highly non-equilibrium conditions seen at the peak of the cascade, the thermal shockwave allows a reference cell method to include lattice distortion in the numbers of defects it

measures. This crystal distortion is part of the process and quite common in thermally activated situations. However, using the reference cell technique shows our results to be coherent with those of Veiller *et al*. Detailed analysis of defect types, specifically antisite defects has shown that the more mobile Ca ions are more likely to end up residing as antisite defects, and this may well be reflected in the large discrepancies between antisite numbers UNZ/ZRZ and CAZ simulations. Other analysis methods used here include asphericity and radius of gyration, which provide extra information suitable for cascade description. Both of these methods proved to be rather insensitive to some physical properties of cascades – representing the overall extent of cascades rather well, but not highlighting the discrepancies in sub-cascade behaviour, defect density or features seen along the central track of a cascade.

Acknowledgements

References

[1] A.E. Ringwood, S.E. Kesson, N.G. Ware, W. Hibberson, A. Major, Nature, 278 (1979) 219-223.

[2] DECC, Management of the UK's Plutonium Stocks, in: D. Department of Energy and Climate Change (Ed.), London, 2011.

[3] F.W. Clinard, American Ceramic Society Bulletin, 65 (1986) 1181-1187.

[4] W.J. Weber, R.C. Ewing, C.R.A. Catlow, T.D. de la Rubia, L.W. Hobbs, C. Kinoshita, H. Matzke, A.T. Motta, M. Nastasi, E.K.H. Salje, E.R. Vance, S.J. Zinkle, Journal of Materials Research, 13 (1998) 1434-1484.

[5] R.C. Ewing, T.J. Headley, Journal of Nuclear Materials, 119 (1983) 102-109.

[6] C. Davoisne, W.E. Lee, M.C. Stennett, N.C. Hyatt, N. Peng, C. Jeynes, Ceramic Transactions, 222 (2010) 3-9.

[7] L. Van Brutzel, M. Rarivomanantsoa, D. Ghaleb, Journal of Nuclear Materials, 354 (2006) 28-35.

[8] H.R. Foxhall, K.P. Travis, L.W. Hobbs, S.C. Rich, S.L. Owens, Philosophical Magazine, Forthcoming (2012).

[9] A. Chartier, C. Meis, J.P. Crocombette, W.J. Weber, L.R. Corrales, Physical Review Letters, 94 (2005).

[10] J.P. Crocombette, D. Ghaleb, Journal of Nuclear Materials, 295 (2001) 167-178.

[11] R. Devanathan, L.R. Corrales, W.J. Weber, A. Chartier, C. Meis, Molecular Simulation, 32 (2006) 1069-1077.

[12] J.A. Purton, N.L. Allan, Journal of Materials Chemistry, 12 (2002) 2923-2926.

[13] K. Trachenko, M.T. Dove, E. Artacho, I.T. Todorov, W. Smith, Physical Review B, 73 (2006).

[14] K.O. Trachenko, M.T. Dove, E.K.H. Salje, Journal of Physics-Condensed Matter, 13 (2001) 1947-1959.

[15] M. Gilbert, J.H. Harding, Physical Chemistry Chemical Physics, 13 (2011) 13021-13025.

[16] J. Mulroue, A.J. Morris, D.M. Duffy, Physical Review B, 84 (2011) 094118.

[17] L. Veiller, J.P. Crocombette, D. Ghaleb, Journal of Nuclear Materials, 306 (2002) 61-72.

[18] F.W. Clinard Jr., L.W. Hobbs, C.C. Land, D.E. Peterson, D.L. Rohr, R.B. Roof, Journal of Nuclear Materials, 105 (1982) 248-256.

[19] M.R. Gilbert, C. Selfslag, M. Walter, M.C. Stennett, J. Somers, N.C. Hyatt, F.R. Livens, IOP Conference Series: Materials Science and Engineering, 9 (2010) 012007.

[20] C. Erginsoy, A. Englert, G.H. Vineyard, Physical Review a-General Physics, 133 (1964) A595-&.

[21] C. Erginsoy, G.H. Vineyard, A. Shimizu, Physical Review, 139 (1965) A118-+.

[22] B.D. Begg, E.R. Vance, S.D. Conradson, Journal of Alloys and Compounds, 271 (1998) 221-226.

[23] E.R. Vance, C.J. Ball, R.A. Day, K.L. Smith, M.G. Blackford, B.D. Begg, P.J. Angel, Journal of Alloys and Compounds, 213 (1994) 406-409.

[24] X. Deschanels, V. Picot, B. Glorieux, F. Jorion, S. Peuget, D. Roudil, C. Jegou, V. Broudic, J.N. Cachia, T. Advocat, C. Den Auwer, C. Fillet, J.P. Coutures, C. Hennig, A. Scheinost, Journal of Nuclear Materials, 352 (2006) 233-240.

[25] R.A. Buckingham, Proceedings of the Royal Society A, Mathematical, Physical and Engineering Sciences, 168 (1938) 264-283.

[26] J.F. Ziegler, J.P. Biersack, U. Littmark, The Stopping and Range of Ions in Solids, Pergamon, New York, 1985.

[27] L. Minervini, R.W. Grimes, Journal of Physics and Chemistry of Solids, 60 (1999) 235-245.

[28] R. Devanathan, L.R. Corrales, W.J. Weber, A. Chartier, C. Meis, Physical Review B, 69 (2004).

[29] W.H. Press, W.T. Vellerling, S.A. Teukolsky, B.P. Flannery, Recipes in Fortran. The art of scientific computing., Cambridge University Press, Cambridge, 1992.

[30] U. Essmann, L. Perera, M.L. Berkowitz, T. Darden, H. Lee, L.G. Pedersen, Journal of Chemical Physics, 103 (1995) 8577-8593.

[31] I.T. Todorov, W. Smith, Philosophical Transactions of the Royal Society of London Series a-Mathematical Physical and Engineering Sciences, 362 (2004) 1835-1852.

[32] H.J. Rossell, Nature, 283 (1980) 282-283.

[33] J.D. Gale, Journal of the Chemical Society-Faraday Transactions, 93 (1997) 629-637.

[34] F.X. Zhang, J. Lian, U. Becker, R.C. Ewing, J. Hu, S.K. Saxena, Physical Review B, 76 (2007).

[35] H. Ozkan, L. Cartz, J.C. Jamieson, Journal of Applied Physics, 45 (1974) 556-562.

[36] I. Todorov, W. Smith, The DL_POLY_3 user manual, in, STFC Daresbury Laboratory, 2007, pp. 104-106.

[37] A.M. Dunn, J. Yates Monteith, M. Bishop, Computers in Education Journal, 18 (2008) 74-81.